Persistent photoinduced magnetization and oxygen non-stoichiometry in $La_{0.9}Ca_{0.1}MnO_3$ films

Persistent photoinduced magnetization and oxygen non-stoichiometry in $La_{0.9}Ca_{0.1}MnO_3$ films

T Suominen[1,2]**, H Huhtinen**[1]**, S Majumdar**[1,3]**, P Paturi**[1]**,
V S Zakhvalinskii**[1,4] **and R Laiho**[1]

[1] Wihuri Physical Laboratory, Department of Physics and Astronomy, University of Turku,
FI-20014 Turku, Finland
[2] Graduate School of Materials Research, Turku, Finland
[3] Department of Physics, Åbo Akademi University, FI-20500 Turku, Finland
[4] Belgorad State University, Pobeda Street 85, 308015 Belgorad, Russia

E-mail: hannu.huhtinen@utu.fi

Abstract
The influence of thermal annealings on $La_{0.9}Ca_{0.1}MnO_3$ (LCMO) films in oxygen and in
vacuum with low hole doping is investigated in the phase separation region where competition
between AFM and FM phases is high. Measurements by x-ray diffractometry, atomic force
microscopy and magnetometry reveal changes in the lattice parameters and magnetic properties
of the films, depending on the oxygen content. All films show magnetic cluster glass properties
with similar freezing temperatures of around 45 K. Clearly the highest increase of the
magnetization is observed in the films annealed in vacuum. We attribute this effect to trapping
of unpaired electrons at oxygen vacancies where they can form rigid self-trapped magnetic
polarons in potential wells of local moments. As a result long-range spin distortions with local
ferromagnetic order may be realized. In conformity with these results, photoinduced persistent
magnetization showing different mechanisms of generation, depending on the method of
thermal annealing, is observed.

(Some figures in this article are in colour only in the electronic version)

1. Introduction

The mixed valence manganites $La_{1-x}M_xMnO_3$ with M = Sr,
Ca, Ba have attracted much interest because of their colossal
magnetoresistance behavior, high spin-polarization of the
ground state and magnetic phase separation. These effects are
governed by Mn^{3+} ($3d^4$, t_{2g}^3, e_g^1)–$O(2p^6)$–Mn^{4+} ($3d^3$, t_{2g}^3) chain
units where e_g electrons can move from Mn^{3+} to neighboring
Mn^{4+} ions due to hybridization of e_g and 2p orbitals [1].
At low values of $x < 0.07$ $La_{1-x}Ca_xMnO_3$ (LCMO) is an
antiferromagnetic (AFM) insulator, between $0.07 < x < 0.22$
it is an insulating ferromagnet (IFM) and for $0.22 < x < 0.5$
it is a ferromagnetic metal (FMM). For $x < 0.125$ small
metallic ferromagnetic (FM) clusters are embedded in the IFM
phase as observed by NMR [2], neutron diffraction [3] and
magnetic measurements [4–6]. The phase separation has been

attributed to bound magnetic polarons (BMPs) [7] formed by
self-trapping of a charge carrier by ferromagnetically oriented
local spins. As proposed recently [8], in two-dimensional (2D)
and three-dimensional (3D) Kondo lattice models the range of
the spin distortions associated with BMP may greatly exceed
the size of the carrier trapping region.

Using magnetic and microwave absorption measurements,
increase of the FMM phase was found in low-doped LCMO
($x < 0.2$) illuminated with red light ($E = 1.59$ eV) at
low temperatures [9]. After switching off the light, the in-
duced magnetization decayed slowly obeying persistent pho-
toinduced magnetization (PPM) behavior [10] which closely
resembles the persistent photoinduced superconductivity in
low-doped $YBa_2Cu_3O_{6+x}$ [11]. The main optical absorption
bands of LCMO are due to the $3d(t_{2g}) \rightarrow 3d(e_g)$ excitations
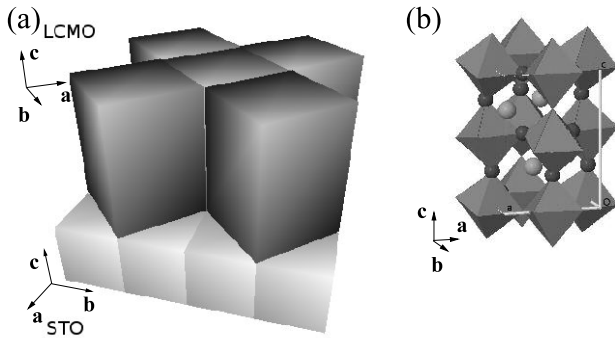with a maximum around 1.5 eV and the $2p(O) \rightarrow 3d(Mn)$

Figure 1. (a) Schematic presentation of the orthorhombic structure of LCMO film on (001) STO and (b) a unit cell of LCMO.

charge transfer transition around 2.4 eV [12]. Our recent measurements of Mn 3p core level spectra in LCMO films give evidence for a decrease of the Mn^{3+} band and an increase of the number of Mn^{4+} ions under illumination with red light according to the reaction [13]

$$Mn^{3+} + Mn^{3+} + h\nu \rightarrow Mn^{4+} + Mn^{2+}. \qquad (1)$$

Electron hopping within the Mn^{3+}–O–Mn^{4+} unit is controlled by oxygen stoichiometry [14]. The oxygen release and absorption lead to lattice expansion or contraction, respectively, due to variations in the Mn ion valence and so the correlation between lattice strain and oxygen content is obvious [15]. Also the magnetic Curie temperature, T_C, saturation magnetization and coercivity are parameters depending on the oxygen content and can be adjusted by annealing treatments [16, 17].

In this work, we investigate the influence of vacuum and O_2 annealing on structural and magnetic properties of LCMO films with $x = 0.1$. In addition, the effect of illumination on O_2 treated and vacuum treated films is studied in order to understand the role of oxygen vacancies in forming of the PPM state. As a control we use an as-deposited film similar to that used in [10].

2. Experimental details

LCMO films of 200 nm thickness were grown on (001) $SrTiO_3$ (STO) substrates by pulsed laser deposition (PLD) using an XeCl excimer laser (as-deposited films A). Details of the material preparation and the film deposition parameters have been reported elsewhere [18–20]. In order to increase or decrease the oxygen content of the films, post-annealing treatments were made in flowing oxygen (sample B) and in vacuum (samples C and D), respectively, using the parameters given in table 1. The (001) STO substrate was chosen to obtain minimal lattice mismatch between the film and the substrate. Depending on the Ca concentration x, the lattice mismatch in LCMO films with $x = 0.1$ grown on (001) STO is +0.5% with tensile strain, while in LCMO with $x = 0.33$ the mismatch is on average +1.0%. In figure 1 is shown the orientation of the LCMO unit cells deposited on (001) STO.

The surface morphology and microstructure of the films were investigated by atomic force microscopy before and after

Table 1. Parameters used in post-annealing treatments of LCMO films on (001) STO substrate.

Sample	Treatment	T (°C)	P (Torr)	Annealing time	Heating/ cooling rate (°C min^{-1})
A	As-deposited	780	0.3	—	—
B	O_2	800	Flowing O_2	24 h	1
C	Vacuum	700	10^{-2}	15 min	10
D	Vacuum	700	10^{-4}	15 min	10

Table 2. The lattice parameters, average peak FWHM widths in 2θ and the difference in unit cell volume (ΔV) as compared to bulk values for the films deposited on (001) STO and after annealings in oxygen (B) at 800 °C and in vacuum at 700 °C (D).

Sample	a (nm)	b (nm)	c (nm)	FWHM (deg)	ΔV (%)
A	0.5477	0.5491	0.7672	0.53	−1.96
B	0.5444	0.5464	0.7691	0.55	−2.78
D	0.5488	0.5499	0.7740	0.63	−0.74

post-annealing treatments. The texturing, lattice parameters and x-ray peak widths were determined from XRD data obtained by a Philips X'pert MPD system with a Schultz texture goniometer using Cu Kα radiation and an incident Ni-filter. On the diffracted beam path a parallel plate collimator with a 0.18° slit and a 0.04 rad Soller slit were used. In detailed scans, the angle resolutions were $\Delta 2\theta = 0.05°$ for the Bragg angle and $\Delta \psi = 0.1°$ for the tilt and rotation $\Delta \phi = 0.1°$ of the sample. Texturing was determined from the ψ-ϕ-scan at (121)/(211) peaks ($2\theta \approx 38.4°$) with $\Delta \psi = \Delta \phi = 3°$ and the lattice parameters and peak widths were observed from detailed 2D 2θ–ϕ-scans over the (121) and (211) peaks. These peaks were chosen to avoid overlapping of the diffraction peaks from the sample and the substrate. The XRD data were analyzed by using a 2D Levenberg–Marquardt fitting [21] of Gaussian peaks. The temperature dependence of the magnetization, M, was measured with a superconducting quantum interference device (SQUID) magnetometer after cooling the sample in zero field (ZFC) or in the measuring field (FC) at temperatures between 5 and 300 K. Magnetic hysteresis curves were recorded in a field of $B = \pm 100$ mT at 5 K. All measurements were made for the sample in the dark or illuminated through an optical fiber using an Ar ion laser working at $\lambda = 514.5$ nm (2.42 eV). The external field B was always oriented along the plane of the films, i.e. along the LCMO [110] axis.

3. Structural and microstructural investigations

3.1. X-ray analysis

XRD analysis revealed no impurity phases and showed full texturing, with the c-axis perpendicular to the film surface (figure 2). The lattice parameters, given in table 2, indicate straining of the films in comparison with the bulk values for $La_{0.9}Ca_{0.1}MnO_3$ at 300 K, $a = 0.548$ nm, $b = 0.551$ nm and $c = 0.778$ nm [22]. The diffraction peak widths (full width at half maximum (FWHM)) for the as-deposited
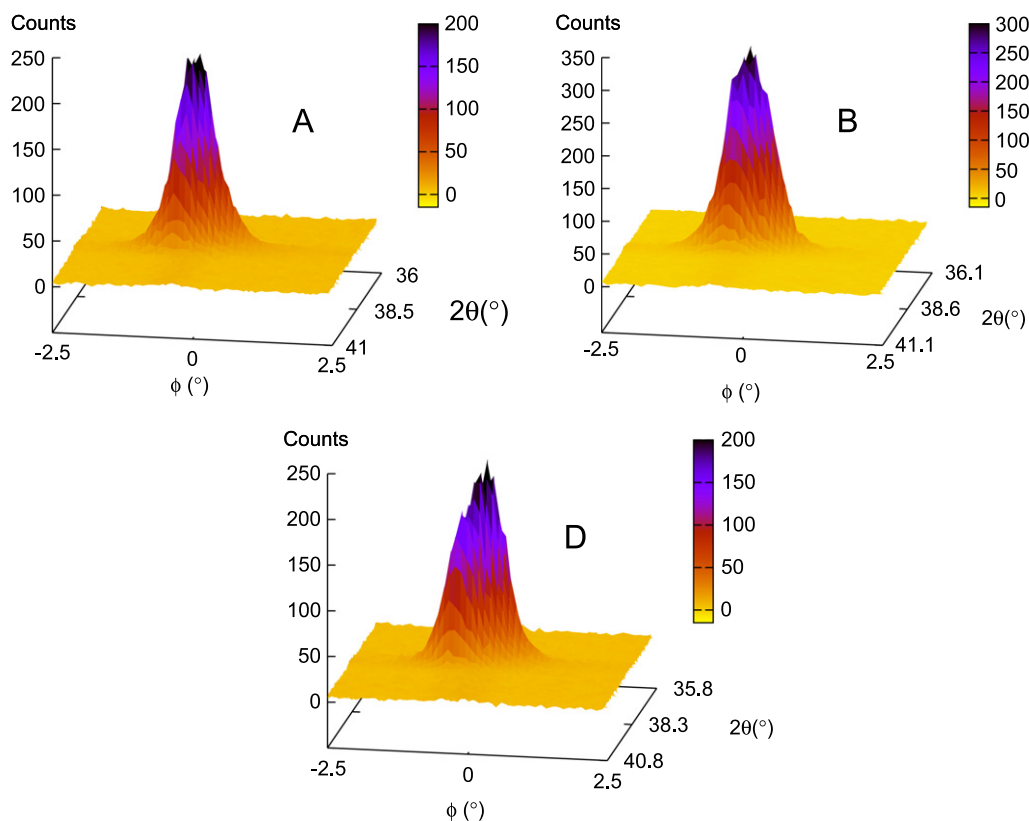
Figure 2. 2θ–ϕ scans over the (211) peaks for LCMO films grown on (001) STO substrates: (A) as-deposited, (B) post-annealed in O_2 and (D) in vacuum.

films exceeded only slightly the instrumental peak widths, indicating a fairly relaxed lattice. As shown in table 2, thermal annealing in oxygen (sample B) adds oxygen in the lattice and contracts the unit cells, whereas annealing in vacuum (C, D) removes oxygen from the lattice and expands the unit cell. Because the perovskite manganites have a stable structure in the oxygen stoichiometric phase [23], the shortening of the lattice parameters can be explained by an increase of the Mn^{4+}/Mn^{3+} ratio by oxygen absorption, since the cation–cation bond is larger than the cation–oxygen–cation bond [24]. As the ionic radius of Mn^{3+} (0.07 nm) exceeds that of Mn^{4+} (0.05 nm), each replacement of Mn^{3+} by Mn^{4+} reduces the volume of the unit cell. To maintain the balance of the charge, each oxygen ion oxidizes two Mn^{3+} ions to Mn^{4+} causing a decrease of 0.04 nm in the lattice parameters. Opposite to this, when oxygen is added in the MnO_6 octahedra, there is an increase of 1/6 i.e. 0.02 nm of oxygen ionic radius (0.12 nm) in the lattice parameter. In the former process, which is more prominent, the lattice parameters decrease with increasing O_2 content. Similarly, release of oxygen from the structure increases the size of the unit cell.

All heat treatments widen the diffraction peaks (table 2) due to more strained lattices and/or differences in the unit cells across the film. As can be seen in figure 2(D), the peak shape changes, especially during vacuum treatment, from a simple Gaussian to a shape with a wide base in the ϕ-scan. The changes due to conversion of Mn^{3+} to Mn^{4+} are likely to be more pronounced at the surface of the film than near

the substrate, where straining of the lattice is stronger. This increases the distribution of the volume and tensile strain in LCMO unit cells. Both of these effects widen the diffraction peaks. It is good to notice that due to the tensile strain by the substrate, the unit cell volume, ΔV, of LCMO is reduced in as-deposited thin film structures when compared to bulk or single crystal values [25]. The ratio of the integrated intensity between the peaks originating from the substrate and from the film are preserved, showing that the film thickness does not change much due to annealing.

3.2. Surface morphology and microstructure

Typical atomic force microscopy images of the LCMO films are shown in figure 3. The films (a) have square shaped grains oriented along the crystallographic [110]-direction of LCMO and show quite good connectivity. The average width of the growth islands is about 300 nm and the grain height on the surface is between 2 and 10 nm. Annealing in oxygen (b) increases the size of the grains, in particular their height is increased up to 50 nm and the islands become roundish and randomly oriented. The samples treated in vacuum (c) have grains of width 100–200 nm which is smaller than in the as-deposited films, while the grain heights are only a couple of nanometers as in the as-deposited films. The basic structure is also smoother, the islands are fused together and are now oriented along the LCMO a/b-axes, having small pores penetrating towards the substrate.
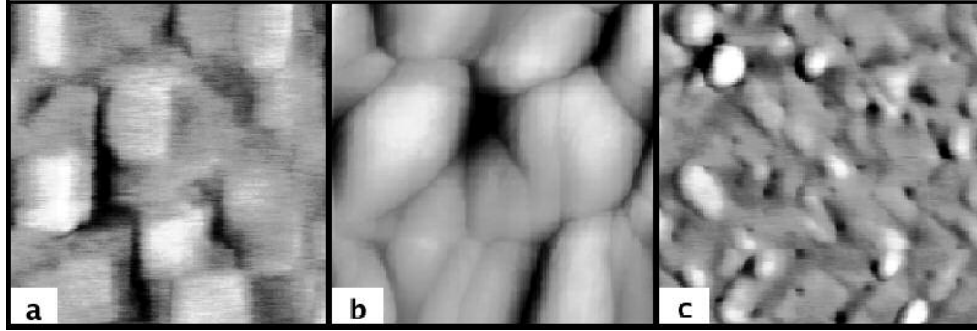
Figure 3. Atomic force microscopy scans of as-deposited (a), O₂ annealed (b) and vacuum annealed (c) LCMO films (table 1). The area of the images is $1 \times 1\,\mu\mathrm{m}^2$ and the grayscales (height from black to white) are 5, 50 and 10 nm for (a)–(c), respectively.

Table 3. Root mean square (rms) roughness and roughness exponent, α, of the LCMO films deposited on STO(001) substrate (A), and after annealing in O₂ (B) and in vacuum (D) (table 1).

LCMO/STO(001)		
Sample	R_{rms} (nm)	α
A	2.5	0.13
B	17.7	0.42
D	1.9	0.09

As shown in table 3 O₂-treatment increases the surface roughness, while annealing in vacuum has a much smaller influence on the morphology of the films. The increase of the surface roughness in the previous case may be ascribed to large inhomogeneities erected upwards from the surface [26]. Values of the surface roughness determined from images can be expressed by the equation [27, 28]

$$R_{\mathrm{rms}}(L, t) = L^{\alpha} f(t L^{-\alpha/g}), \qquad (2)$$

where L is the length over which the roughness is measured, t is the time and α and g are the roughness and growth exponents, respectively. Because we are interested in static roughness, t is much longer than the saturation time $t_{\mathrm{sat}} \propto L^{\alpha/g}$, and so we can write $R_{\mathrm{rms}} \propto L^{\alpha}$. The R_{rms} values are given in table 3 together with α, which usually varies for thin manganite films between 0.4 and 0.6. The relatively small values of α indicate that our films are not nucleated with a pure 3D island growth mode but approach monolayer to monolayer growth [29–31]. The differences in annealing times (table 1) are most likely responsible for variations of the values of α.

4. Magnetic properties

4.1. Temperature and magnetic field dependences

As shown previously, in La$_{0.9}$Ca$_{0.1}$MnO$_3$ the amount of FMM phase inside the IFM matrix can be increased by illumination with light [9, 10]. In the present work we discuss the influence of post-deposition annealing in oxygen or in vacuum on structural and magnetic properties of La$_{0.9}$Ca$_{0.1}$MnO$_3$ films in dark and under illumination. The as-deposited samples (A) are similar to those studied in [10] and are presented here for comparison. The $M_{\mathrm{ZFC}}(T)$ and $M_{\mathrm{FC}}(T)$ curves
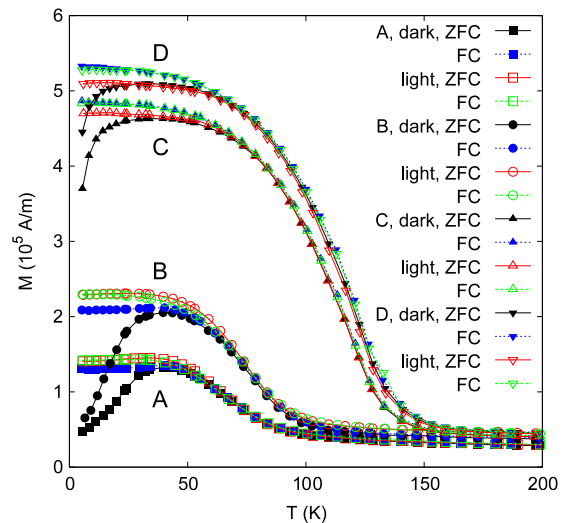

Figure 4. Temperature dependence of M_{ZFC} and M_{FC} ($B = 20$ mT) measured before and during illumination of the films. The solid symbols refer to measurements in the dark and the open symbols to those made under illumination with the 514.5 nm wavelength of the Ar ion laser.

shown in figure 4 are found to deviate from each other at a temperature depending on the way of cooling the sample (ZFC or FC in 20 mT field) or whether it was illuminated or not before the measurements. In unilluminated samples A and B there is a broad maximum in the $M_{\mathrm{ZFC}}(T)$ curves around a freezing temperature, $T_{\mathrm{f}} \approx 45$ K, below which the difference of $M_{\mathrm{FC}}(T) - M_{\mathrm{ZFC}}(T)$ starts to deviate from zero while $M_{\mathrm{FC}}(T)$ is almost temperature independent. This kind of behavior is typical of magnetic cluster glasses with weak intercluster interactions which can be confirmed by ac susceptibility measurements. In comparison with the as-deposited film, the magnetization is nearly doubled in the film B while T_{f} is shifted only slightly. This means increasing of the number of magnetic clusters in film B with similar moments as in film A. As a result of illumination, the value of the difference $M_{\mathrm{FC}}(T) - M_{\mathrm{ZFC}}(T)$ which is related to anisotropy of the shape and orientation of magnetic clusters becomes zero due to growth of $M_{\mathrm{ZFC}}(T)$ at $T < T_{\mathrm{f}}$. As shown in table 4, the magnetic Curie temperature T_{C} of the as-deposited film A is 89 K. Annealing the film in oxygen

Table 4. Curie temperature, coercive field (B_c) and the ratio of maximum magnetization M_{max} and the remanent magnetization M_{rem} of the films before and during illumination are calculated from the temperature dependence of M and the hysteresis loop curves shown in figures 4–6.

Film	Unilluminated			Illuminated		
	T_c (K)	$B_{c,5K}$ (mT)	M_{rem}/M_{max} (%)	T_c (K)	$B_{c,5K}$ (mT)	M_{rem}/M_{max} (%)
As-deposited	89	17	35	89	0	14
Oxygen	100	24	42	100	0	17
Vacuum 1	146	8	38	146	3	35
Vacuum 2	152	3	62	152	3	58

(sample B) rises the value of T_C to 100 K and increases the magnetization. Similar enhancements of $M(B)$ and T_C have been observed in oxygen annealed $La_{0.7}Ca_{0.3}MnO_3$ films [17] and in $La_{0.84}Ca_{0.16}MnO_{3-\delta}$ films where these changes were related to an increase of the ratio Mn^{4+}/Mn^{3+} [32].

The virgin $M(B)$ curves, measured at 5 K up to $B = 100$ mT are shown in figure 5. Although the as-deposited and the oxygen treated films show practically linear field dependence without illumination, vacuum annealings result in FM type virgin curves. The linear initial magnetization curve $M(B)$ presented for films A and B in figure 5 in dark and the slight upturn seen after illumination can be attributed to competition between AFM and FM domains [33]. After the first vacuum treatment (film C) the magnetization is not yet saturated at $B = 100$ mT. The second vacuum treatment (film D) leads to a steeper increase of the $M(B)$ curve than observed in the as-deposited and oxygen treated films and the magnetization is nearly saturated around $B = 100$ mT. Because we have not found any impurity phases in these films and according to surface analysis shown in figure 3 there is a clear difference in the size of the grains, we could explain the differences between the samples by the magnetic domain size and by the size and movements of domain walls in similar oxides [34, 35].

According to our XPS results [13] on pristine $La_{1-x}Ca_x$ MnO_3 ($x < 0.2$) films illuminated with red light, manganese ions can adopt 2+, 3+ and 4+ valence states (see equation (1)). This suggests a competition of FM coupled double exchange pairs $Mn^{3+}-Mn^{2+}$ and $Mn^{3+}-Mn^{4+}$ with AFM coupled super-exchange pairs $Mn^{3+}-Mn^{3+}$ and $Mn^{2+}-Mn^{2+}$ in defining the nature of the magnetic phase [36]. The inhomogeneity caused by differently coupled Mn–Mn pairs increases the spin disorder, resulting in local magnetic fluctuations which may lead to an increased number of small FMM clusters.

In figure 6 are shown the magnetic hysteresis loops measured at 5 K between -100 and 100 mT for the films (A–D). The oxygen annealed film (B) has the most open loop, in terms of the coercivity field, B_C, and annealing in vacuum (C–D) shrinks and sharpens the loop. After the first vacuum treatment (C), the magnetization is not saturated in the low field region as observed after the second vacuum treatment (D). In as-deposited and oxygen treated films A and B the hysteresis loops can be closed completely by illumination, but the vacuum annealed films are much less influenced. The sample A behaves similarly to the as-deposited samples in [10]. The values of B_C and the ratio of M_{rem}/M_{max} (100 mT) are shown
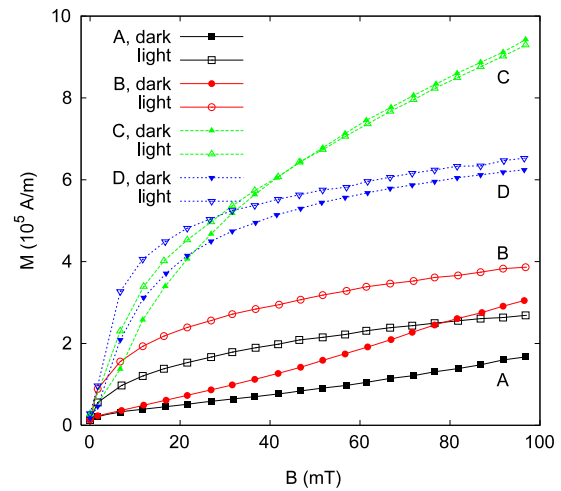

Figure 5. Virgin magnetization curves observed at 5 K for all the films before (solid symbols) and during (open symbols) illumination.

in table 4. It is noteworthy that when the FM component has been increased by vacuum annealing, the photoinduced effect is much smaller or even lacking (D), because the maximum ferromagnetism has already been reached by the optimum Mn^{4+}/Mn^{3+} ratio induced in vacuum treatment [32, 37]. As shown in figures 2 and 5, the corresponding changes are seen also in the XRD and in the virgin curve measurements. Large surface roughness of O_2-annealed films indicates the presence of more defects in the films that may act as magnetic pinning sites and therefore increase the coercive field [38]. This is in accordance with our atomic force microscopy results (table 3) showing that the oxygen treated films have the largest surface roughness and highest B_C without illumination (table 4, figures 6(c) and (d)).

4.2. Photoinduced persistent magnetization

As shown by the solid lines in figure 7 the growth and relaxation of the persistent photoinduced magnetization PPM can be fitted with a stretched exponential law known as the Kohlrausch expression,

$$M_{ill}(t) = M_{ill}^{sat} \exp[-(t/\tau)^\beta], \quad (3)$$

where $\tau(T, B)$ is a characteristic time and the exponent β is a dispersion parameter $0 < \beta < 1$. Comparison for vacuum treated samples is made by using our earlier data
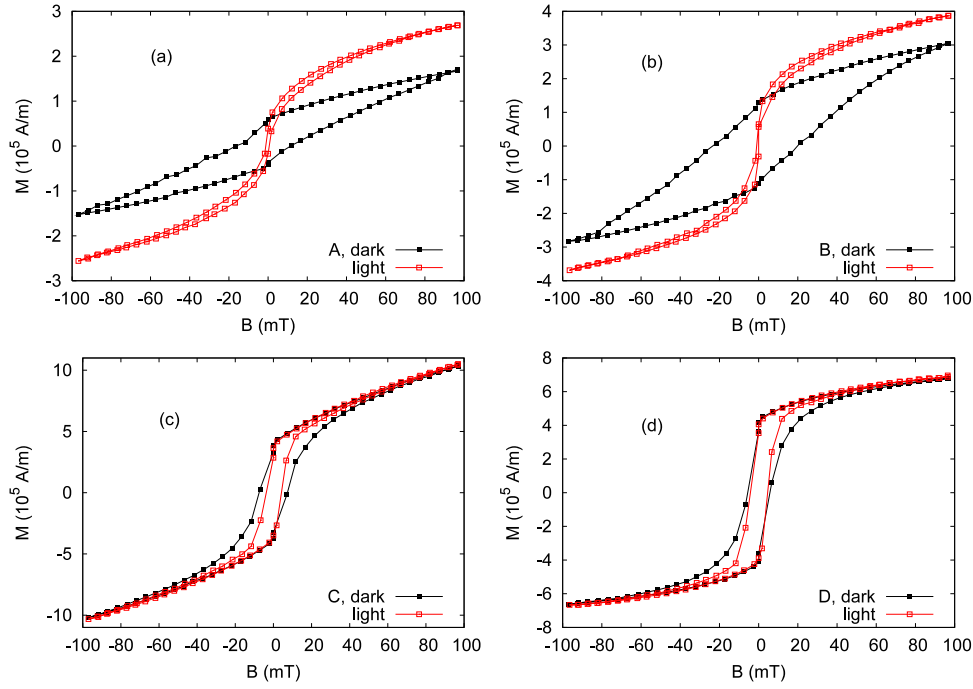
Figure 6. The hysteresis loops measured at 5 K between −100 and 100 mT on as-deposited, oxygen annealed and vacuum annealed films (C and D) and (d) before (solid symbols) and during (open symbols) illumination.
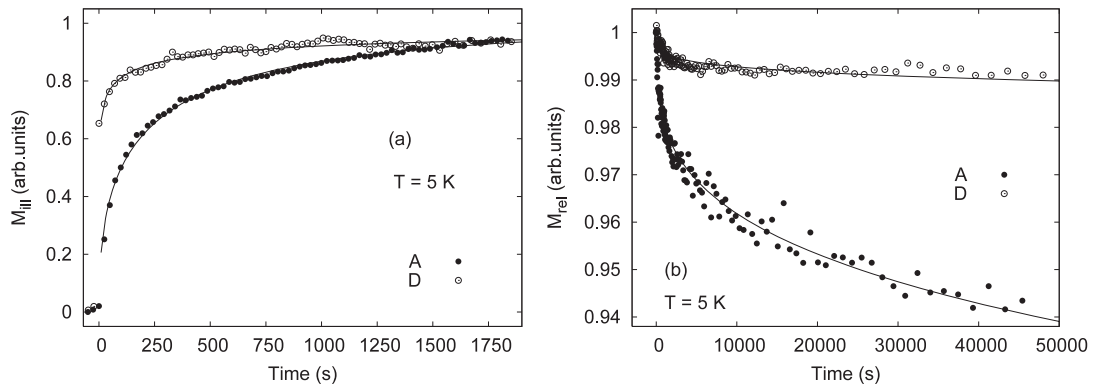

Figure 7. Time dependence of the growth of photoinduced magnetization, M_{ill}, at 5 K and $B = 20$ mT for as-deposited (A) and vacuum annealed (D) LCMO films (a) and the relaxation of the PPM state (b). The solid lines show fits with the stretched exponential law (3).

in the as-deposited film of [10]. The exponents β_g and β_r (indices g growth and r relaxation) in equation (3) are related to growth and relaxation of the PPM, respectively. These exponents have been analyzed earlier in detail for as-deposited La$_{0.9}$Ca$_{0.1}$MnO$_3$ films [10] and the value of $\beta_g \approx 0.43$ in a 20 mT field used in this work is close to the 3/7 predicted for charge transfer processes induced by phonons in the presence of randomly distributed traps [39]. For the vacuum annealed film D we find a clearly smaller exponent $\beta_g = 0.18$. For relaxation of M_{ill} in film A the value of $\beta_r = 0.3$ is found and for the vacuum annealed film D we get $\beta_g = 0.18$ and $\beta_r = 0.29$ corresponding to the relaxation of M_{ill} with $\beta_r = 0.3$ in film A. The time dependence of PPM observed in LCMO resembles the photoinduced superconductivity in oxygen-deficient YBa$_2$Cu$_3$O$_x$ films [11, 40] where the photoexcited electrons are believed to be trapped at oxygen

vacancies in oxygen chains, hindering the recombination of electrons with photoholes located in the superconducting CuO$_2$ planes [41]. Slowly relaxing resistivity has been reported also in illuminated (La, Ca) MnO$_\delta$ films.

5. Discussion

Increasing of the oxygen annealing temperature of optimally hole doped-La$_{0.67}$Ca$_{0.33}$MnO$_{3-\delta}$ usually increases the values of M and T_C [42]. In comparison with the $\delta = 0$ films, our as-deposited films with $T_C < 100$ K are oxygen deficient and have a large AFM component. On the other hand, when $\delta < 0$ the lattice decreases the value of T_C and broadens the magnetic transition region because of increased lattice disorder [42]. Also significant differences have been observed in the values of M and the transition widths for LCMO with $\delta = 2.90$

and 2.85 [38]. A simple calculation gives in $La_{0.9}Ca_{0.1}MnO_3$ the ratio of Mn^{3+}/Mn^{4+} as 9:1. This means that only about 20% of the Mn–O–Mn bridges contain FM coupled Mn^{3+}–O–Mn^{4+} pairs while the rest are in the AFM coupled Mn^{3+}–O–Mn^{3+} pairs. As can be concluded from table 1 and figure 5, annealing the as-deposited films in oxygen at a sufficiently high temperature ($\approx 800\,^\circ$C) raises the values of M and T_C.

Vacuum annealing is a reducing process which can lead in LCMO films with Ca ($x = 0.33$) to a strain-dependent release of oxygen from the lattice [15]. An increase of Mn^{2+} concentration has been observed by x-ray absorption spectroscopy (XAS) and x-ray photoelectron spectroscopy (XPS) measurements when oxygen vacancies are formed by vacuum annealing [43]. Because most Mn–O–Mn pairs are AFM coupled in low-doped LCMO, the charge transformation in the vacuum annealed samples can produce more Mn^{4+} ions by hole formation, in agreement with the measurements of M in figure 5. In thin films the surface effect is remarkable and the presence of dynamic Mn^{2+} can be understood by the valence instability of the Mn^{3+} ions which creates both Mn^{4+} and Mn^{2+} species [43]. Our results give evidence that short term vacuum annealing at moderate temperature ($700\,^\circ$C) is a more effective way to increase the FM phase in low-doped LCMO films than long term annealing at higher temperatures in oxygen. Observation of ferromagnetism has been reported in nanoparticles of several oxides where oxygen deficiency results from film growth conditions without using any doping [44] as well as in HfO_2, TiO_2 and In_2O_2 films [45]. It has been suggested that ferromagnetism in oxide compounds may be formed by trapping of unpaired electrons at oxygen vacancies (F-center mechanism) [46].

The clear difference of β_g for the films A (0.46) and D (0.18) gives evidence that the growth of PPM in these two types of films is governed by different mechanisms. A small value of β_r has been associated with short-range relaxational channels formed by spatial inhomogeneities [47] in a sample. Our results suggest that in the D film a large number of oxygen vacancies potentially able to trap electrons are created. Photoinduced changes in microwave permittivity give evidence for the expansion of the FMM phase in low-doped LCMO under illumination [9]. The spin of the trapped electron (ferron core) [7, 48] has been predicted to form in manganites a rigid self-trapped magnetic polaron consisting of a ferromagnetic core surrounded by spin distortions decaying in the 3D case as a^4/r^4 where a is the radius of the magnetic polaron and r is the distance [8]. This process is in accordance with increase of ferromagnetism in our oxygen-deficient manganites.

The magnetoresistance manganites can be regarded as charge transfer materials with a value of band gap of the order of a few electron volts [49] where the states of O and Mn ions should be defined by some order of covalency. It is generally believed that electronic excitations in oxides containing 3d cations are transferred from oxygen to metal cations. In agreement with experimental observations [12], analysis of one center transitions in manganites [50] suggests that there exist O 2p–Mn 3d dipole transitions with broad absorption bands between 1.2 and 3.2 eV with maxima around 2.0 eV, allowing transfer of an electron into Mn^{3+}.

The hole located in a non-bonding 2p orbital can interact ferromagnetically with the 5d shell. As a result, a nominally Mn^{2+} ground state would be formed in agreement with equation (1) and contribute to an increase of the FM phase in the sample. This process is supported by observations of persistent photoinduced magnetization M_{ill} in our samples with growth exponent 0.46 in equation (3), matching well with the value of 3/7 predicted for charge transfer processes [39]. Such an approach would allow the transfer of an electron from oxygen to the Mn^{3+} ion forming a double exchange interaction pair Mn^{2+}–O–Mn^{3+} which can contribute to an increase of the FM phase. This mechanism may be involved in the A and B films containing oxygen but would be strongly reduced in the vacuum annealed samples, in agreement with our experimental results.

6. Conclusions

Structural and magnetic properties $La_{0.9}Ca_{0.1}MnO_3$ films are investigated before and after subjecting them to post-deposition thermal annealings in oxygen atmosphere or in vacuum. Compared with the as-deposited films, increasing the oxygen by thermal annealing practically doubles the magnetization of the films while the magnetic cluster glass behavior shown in the original films below 100 K is preserved. Even a much stronger increase of the magnetization can be obtained by annealing the films in vacuum. This behavior is attributed to an increased number of oxygen vacancies capable of trapping single electrons to form self-trapped magnetic polarons with neighboring moments.

Persistent photoinduced magnetization, excited by green light is observed in the as-deposited and in oxygen annealed LCMO films in external magnetic field. In this spectral region strong dipole-allowed O 2p–Mn 3d charge transfer transitions occur. The photoinduced magnetization is explained by the non-bonding oxygen 2p hole having a wide orbit and ferromagnetic interaction with the Mn 3d shield. The ground state of this excitation is a high-spin Mn^{2+} state, in conformity with equation (1). This process is supported by the observation that in vacuum annealed LCMO samples depleted of oxygen the photoinduced magnetization M_{ill} is weak or completely missing. Also the growth exponent $\beta_g = 0.46$ of the stretched exponential law in equation (3) for M_{ill} agrees with the prediction 3/7 for charge transfer systems.

Acknowledgments

References

[1] Tokura Y 2000 *Colossal Magnetoresistance Oxides* (New York: Gordon and Breach)
[2] Allodi G, Guidi M C, Renzi R D, Caneiro A and Pinsard L 2001 *Phys. Rev. Lett.* **87** 127206
[3] Hennion M, Moussa F, Biotteau G, Rodriguez-Carvajal J, Pinsard L and Revcolevschi A 1998 *Phys. Rev. Lett.* **81** 1957
[4] Papavassiliou G, Fardis M, Belesi M, Maris T G, Kallias G, Pissas M and Niarchos D 2000 *Phys. Rev. Lett.* **84** 761

[5] Laiho R, Lähderanta E, Salminen J, Lisunov K G and
    Zakhvalinskii V S 2001 *Phys. Rev.* B **63** 94405
[6] Markovich V, Fita I, Puziniak R, Tsindlekht M I,
    Wisiniewski A and Gorodetsky G 2002 *Phys. Rev.* B
    66 094409
[7] Dagotto E 2003 *Nanoscale Phase Separation and Colossal
    Magnetoresistance: the Physics of Manganites and Related
    Compounds* (Berlin: Springer)
[8] Ogarkov S L, Kagan M Y, Sboychakov A O,
    Rakhmanov A L and Kugel K I 2006 *Phys. Rev.* B
    74 014436
[9] Huhtinen H, Laiho R, Lähderanta E, Vlasenko L,
    Vlasenko M P and Zakhvalinskii V 2000 *Phys. Rev.* B
    62 11614
[10] Huhtinen H, Laiho R and Zakhvalinskii V 2005 *Phys. Rev.* B
    71 132404
[11] Kudinov V I, Chaplygin I L, Kirilyuk A I, Kreines N M,
    Laiho R, Lähderanta E and Ayache C 1993 *Phys. Rev.* B
    47 9017
[12] Lawler J F, Lunney J G and Coey J M D 1994 *Appl. Phys. Lett.*
    65 3017
[13] Huhtinen H, Laiho R, Vlasenko L S, Vlasenko M P,
    Zakhvalinskii V, Leiro J, Mattila S, Sutara F and
    Vondracek M 2008 *J. Magn. Magn. Mater.* **320** 1747
[14] Du Y S, Wang B, Li T, Yu D B and Yan H 2006 *J. Magn.
    Magn. Mater.* **297** 88
[15] Sun J R, Yeung C F, Zhao K, Zhou L Z, Leung C H,
    Wong H K and Shen B G 2000 *Appl. Phys. Lett.* **76** 1164
[16] Dho J, Hur N H, Kim I S and Park Y K 2003 *J. Appl. Phys.*
    94 7670
[17] Li T, Wang B, Dai H, Du Y, Yan H and Liu Y 2005 *J. Appl.
    Phys.* **98** 123505
[18] Huhtinen H, Paturi P, Lähderanta E and Laiho R 1999
    Supercond. Sci. Technol. **12** 81
[19] Huhtinen H, Järvinen J, Laiho R, Paturi P and Raittila J 2001
    J. Appl. Phys. **90** 1521
[20] Huhtinen H, Raittila J, Paturi P, Salminen J and
    Zakhvalinskii V S 2002 *J. Phys.: Condens. Matter* **14** 7165
[21] Press W H, Flannery B P, Teukolsky S A and
    Vetterling W T 1990 *Numerical Recipes in C: the Art of
    Scientific Computing* (Cambridge: Cambridge University
    Press)
[22] Dai P, Zhang J, Mook H A, Foong F, Liou S H,
    Dowben P A and Plummer E W 1996 *Solid State Commun.*
    100 865
[23] Worledge D C, Snyder G J, Beasley M R, Geballe T H,
    Hiskes R and DiCarolis S 1996 *J. Appl. Phys.* **80** 5158
[24] Goodenough J B 1955 *Phys. Rev.* **100** 564
[25] Vengalis B, Maneikis A, Anisimovas F, Butkute R,
    Dapkus L and Kindurys A 2000 *J. Magn. Magn. Mater.*
    211 35
[26] Berndt L M, Balbarin V and Suzuki Y 2000 *Appl. Phys. Lett.*
    77 2903
[27] Krim J and Indekeu J O 1993 *Phys. Rev.* E **48** 1576
[28] Palasantzas G and Krim J 1994 *Phys. Rev. Lett.* **73** 3564
[29] Tong W M, Williams R S, Yanase A, Segawa Y and
    Anderson M S 1994 *Phys. Rev. Lett.* **72** 3374
[30] Ramirez J G, Perez F, Gomez M E and Prieto P 2004 *Phys.
    Status Solidi* c **1** S13
[31] Ghosh B, Brar L K, Jain H, Mitra J and
    Raychaudhuri A K 2004 *J. Phys. D: Appl. Phys.* **37** 1548
[32] Seo D, Kang H C, Jang H W and Noh D Y 2005 *Phys. Rev.* B
    71 12412
[33] Heck C 1974 *Magnetic Materials and their Applications*
    (London: Butterworths)
[34] Gonzalez O J, Castano E and Gracia F J 2002 *Vacuum* **64** 321
[35] Joy P A and Date S K 2000 *J. Magn. Magn. Mater.* **218** 229
[36] de Gennes P G 1960 *Phys. Rev.* **118** 141
[37] de Jong M P, Dediu V A, Taliani C and Salaneck W R 2003
    J. Appl. Phys. **94** 7292
[38] Du Y S, Wang B, Li T, Yu D B and Yan H 2006 *J. Magn.
    Magn. Mater.* **297** 88
[39] Phillips J C 2000 *Physica* C **340** 292
[40] Osquiguil E, Maenhoudt M, Wuyts B, Bruynseraede Y,
    Lederman D and Schuller I K 1994 *Phys. Rev.* B **49** 3675
[41] Hao J, He G, Lu D and Wong H K 2000 *Mater. Lett.* **46** 225
[42] Dabrowski B, Klamut P W, Bukowski Z, Dybzinski R and
    Siewenie J E 1999 *J. Solid State Chem.* **144** 461
[43] de Jong M P, Bergenti I, Dediu V A, Fahlman M, Marsi M and
    Taliani C 2005 *Phys. Rev.* B **71** 014434
[44] Sundaresan A, Bhargavi R, Rangarajan N, Siddesh U and
    Rao C N R 2006 *Phys. Rev.* B **74** 161306(R)
[45] Hong N H, Sakai J, Poirot N and Brize V 2006 *Phys. Rev.* B
    73 132404
[46] Vinokurov I, Zonn Z and Ioffe V 1968 *Sov. Phys.—Solid State*
    9 2659
[47] Phillips J C 1996 *Rep. Prog. Phys.* **59** 1133
[48] Nagaev E L 2001 *JETP Lett.* **74** 431
[49] Coey J M 2001 *J. Alloys Compounds* **326** 2
[50] Moskvin A S 2002 *Phys. Rev.* B **65** 205113